Development and implementation of a device for $LiFePO_4$ batteries state-of-charge estimation

Francisco M. R. Bota

***Abstract*—In this paper, a new SOC (State-Of-Charge) estimation technique, based on the internal impedance of a $LiFePO_4$ battery and fuzzy logic, is proposed.**

The frequency response of a $LiFePO_4$ battery cell, representing its internal impedance, is acquired from an electrochemical impedance spectroscopy (EIS). This acquired variable has a non-linear relationship to SOC, thus, an adaptive methodology approach is taken. The result of the EIS measurement renders the input to a fuzzy logic system designed for the battery SOC estimation, through a comparative analysis between the current impedance measurement and previously observed ones, related to certain values of SOC. To attain this comparative analysis, the fuzzy inference model is previously constructed using an adaptive neuro-fuzzy inference system (ANFIS) technique, based on past EIS measurements, for pre-defined SOC values.

A device is developed, using the Arduino Due platform and an assembled printed circuit board (PCB), so that both processes mentioned above are implemented. The results proved that the implemented system is capable of correctly inferring the battery SOC, although being highly dependent on the amount of past information being acquired, modelling the fuzzy inference system.

***Index Terms*–LiFePO4 battery, SOC estimation, EIS, Internal impedance, ANFIS, Fuzzy Logic, Arduino Due.**

I. Introduction

With the rise of autonomous applications in the past years and its predicable growth in the forthcoming ones, comes the ascent of energy storage systems demand. The progress in energy efficiency and the decline of non-renewable sources of energy dictates the advancement in battery monitoring systems. With this in mind, an accurate and reliable measurement of a battery state-of-charge (SOC) is of the most priority to its active management. The SOC value describes the available stored energy in the battery in relation to its full capacity. This indicator is not only relevant from the remaining capacity point of view but also of extreme importance to the lifetime of the monitorized battery seeing that these systems are sensitive to deep discharges or overcharges related to high or too low SOC values, states capable of irreversible damaging the battery. A battery system, depending on the application, is usually composed of more then one cell. With this, rises another problem, related to the different usage times for each cell, seeing that in these cases, SOC is measured for the entire set of cells. This uneven usage leads to rapid ageing of some cells resulting in its destruction, thereby decreasing the lifetime of the entire pack. Therefore, battery SOC estimation methods are of great importance.

This work aims the implementation of a reliable and automatic SOC measurement system. The ultimate goal is to this in a compact and low-cost way.

Lithium iron phosphate ($LiFePO_4$ or LFP) battery cells are emerging as a choice when a long cycle life and safety supersedes energy density, such as in electric vehicles. This work addresses the development of a system capable of measuring the SOC value of $LiFePO_4$ cells. In that context, the proposed sytem will be able to measure the impedance profile of a given cell, through the development of an EIS measurement system, later inferring its SOC value using an adaptive neuro-fuzzy methodology. The implemented system will automatically estimate this variable based on previous acquired cell impedance profile measurements.

The paper is divided in the following sections: 1) the concept where the proposed method is explained; 2) the detailed implementation of the SOC estimating system de 3) the analysis of the developed system using a $LiFePO_4$ cell as test subject.

II. The State of Charge (SOC) Estimating Method

The ratio of the amount of electrical energy stored in a cell ($Q(t)$) to its maximum capacity (Q_n) is usually referred to as the state-of-charge (SOC) of the cell. It can be defined as follows:

$$SOC(t) = \frac{Q(t)}{Q_n} \tag{1}$$

The SOC of the battery is a non-linear function depending on various parameters. Some variables affecting the SOC are temperature, charge-discharge rates, hysteresis, self-discharge, and cell age [1]. Several approaches have been proposed for the SOC estimation and some [2–5] allow a division into three main estimator categories: the direct, the indirect or book-keeping methods, and finally adaptive systems for SOC estimation.

Direct measurement methods concern the measurement of battery variables and later relating them to SOC. These include the battery voltage (V), battery impedance (Z) and voltage relaxation time (τ) when a current step is applied. Direct methods include the open circuit voltage method, the EMF method and the impedance measurement method.

Indirect SOC measurement methods, or book-keeping methods, are based on coulometric systems, measuring and integrating the battery charging/discharging current.

The uncertainty of the battery and its management system behaviour, due to the influence of previously mentioned parameters, is the main problem to an accurate SOC estimation. For this reason, adaptive systems based on Fuzzy Logic, Artificial Neural Network (ANN) and Kalman Filter(KF) combined with direct measurements, indirect measurements or both, offer a better solution for on-line SOC estimation. The method presented in this paper follows this approach, combining the internal impedance of the cell, acquired from EIS, with fuzzy logic, in order to estimate its SOC value.

A. Electrochemical impedance spectroscopy (EIS)

Electrochemical impedance spectroscopy (EIS) is an experimental technique with the purpose of characterizing electrochemical systems as a function of frequency. This method measures the impedance of a system over a defined range of frequencies, hence the frequency response of the system. The impedance data obtained by EIS is usually represented graphically in a Nyquist plot or a Bode plot.

Impedance is measured in potentiostatic mode or galvanostatic mode. In potentiostatic mode, an AC potential is imposed to a cell and its response current is measured. In galvanostatic mode, impedance is measured imposing an excitation current to the cell, thereby measuring its response potential. In galvanostatic mode, the excitation current, as a function of time, using Eulers relationship, is stated as:

$$i(t) = I_0 \exp(j\omega t) \tag{2}$$

where $i(t)$ is the current at the time instant t, I_0 is the amplitude of the signal, and ω is the angular frequency.

The response signal, $u(t)$, is shifted in phase (ϕ) and has an amplitude U_0:

$$u(t) = U_0 \exp(j(\omega t + \phi)) \tag{3}$$

Accordingly, the impedance is represented in the complex plane as:

$$\overline{Z} = \frac{V_0 \exp(j(\omega t + \phi)}{I_0 \exp(j\omega t)} = Z_0 \exp(j\phi) \tag{4}$$

B. Fuzzy logic applied to a system with two inputs using learning examples

Sometimes, it is not the best practice to establish the IF-THEN rules of a fuzzy system using a human operator. Frequently, one cannot discern what the membership functions should look like simply from observing the data. In other cases, the option of inferring the fuzzy output through a comparative analysis between the current inputs and previous ones, representing the behaviour of the system, is preferred. In these cases, the output of a given system is accomplished using a technique that provides a method for the fuzzy modelling procedure to learn information about a previously acquired data set, rather than choosing randomly the membership function parameters. Hence, for systems to which already exists a collection of input/output data, neuro-adaptive techniques incorporated with fuzzy logic are used in order to compute the membership function parameters that best allow the associated fuzzy inference system to track the current input/output data. This is the idea behind ANFIS or adaptive neuro-fuzzy inference systems, so that a membership function parameter adjustment is attained [6].

In this paper, this learning technique associated to the neuro-fuzzy inference system is applied to the input/output data, resulting from the EIS implemented system presented in the next chapter, through the Fuzzy Logic Toolbox function existent in MATLAB. This function works by introducing as an argument an input/output data set so that the toolbox function named anfis constructs a fuzzy inference system (FIS) output file in which the membership function and singleton parameters associated with each rule are adjusted automatically. This way, a model describing the impedance spectra database is created, containing the mentioned parameters, so that an IF-THEN rule based fuzzy inference system is later implemented.

III. Implementation of the EIS measurement and SOC estimation systems

In this chapter the implementation of the proposed EIS measurement system is described. In addition, the adopted solution applied to the $LiFePO_4$ battery cell SOC estimation, describing the use of ANFIS methodology previously introduced, is delineated.

The proposed system combines signal generation, acquisition, processing and SOC estimation. It is composed by three main blocks, displayed in Figure 1:

- An Arduino Due, providing a variable frequency voltage source (DDS and DAC in Figure 1).
- A customized PCB (Printed Circuit Board):
  - First filtering the input signal from the voltage source Arduino (LP and HP filter in Figure 1).
  - Afterwards, amplifying the signal using a linear voltage-controlled current source (VCCS), producing a sinusoidal excitation current applied to the cell (Enhanced Howland current source in Figure 1).
  - Finally, acquiring both voltage and current signals, using a hall sensor and two external analog-to-digital converters (Hall sensor and ADCs in Figure 1).
- Another Arduino Due microcontroller, responsible for the signals processing and SOC estimation:
  - Firstly, imposing the sampling frequency to the external ADCs located in the PCB.
  - Simultaneously, storing the acquired samples resulting from the ADC conversion, while applying oversampling and moving average filtering techniques (Oversampling and Averaging; Moving Average Filter in Figure 1).
  - Proceeding this, applying the Discrete Fourier transform to both voltage and current in order to obtain the impedance spectra of the cell (DFT blocks in Figure 1).
  - Finally, inferring the SOC value, employing the ANFIS methodology (ANFIS block in Figure 1).

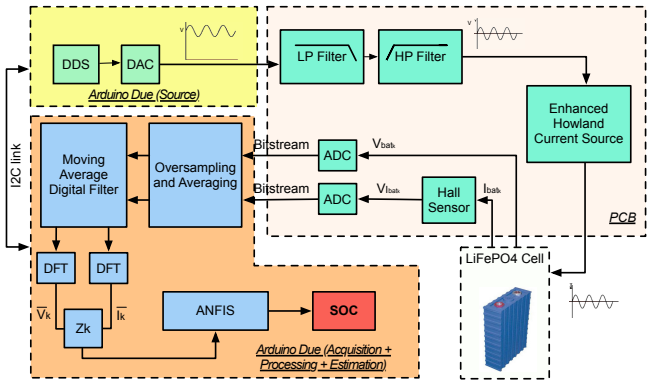

Fig. 1: Block diagram of the proposed EIS measurement and SOC estimation systems.

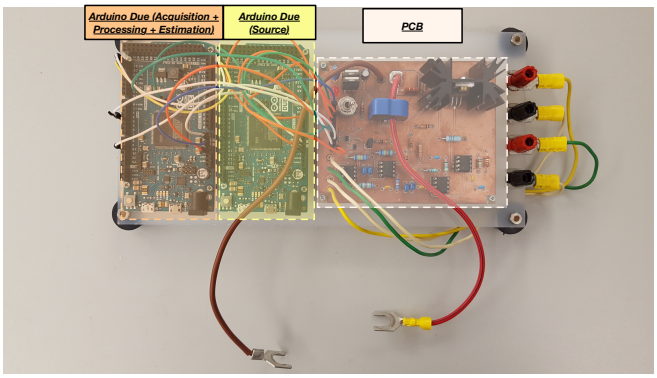

Fig. 2: Developed device composed by three main bocks: Arduino Due (source), PCB and Arduino Due (responsible for the signal acquisition, processing and SOC estimation).

A. Arduino Due

Both signal generation and signal acquisition were executed using a commercial Arduino Due platform. The Arduino Due is a microcontroller board embedding a 32-bit ARM core microcontroller (Atmel SAM3X8E), being clocked at 84 MHz. It embeds a dual channel 12-bit digital to analog converter (DAC) output, 16 12-bit analog to digital converter (ADC) inputs, 54 digital pins that can be used as an input or output. Each pin is able to provide a current of 3 mA or 15 mA, depending on the pin, or receive a current of 6 mA or 9 mA, depending on the pin. The Due has 512 KB of flash memory, where the Arduino sketch is stored, and 96 KB of SRAM, where the sketch creates and manipulates variables while it runs.

In this project, two Arduino Due were employed and a firmware has been developed for each, one for the variable frequency voltage source and another one for the cell impedance measurement system in addition to the SOC inference system based on the measured impedance data.

B. Variable frequency voltage source

In order to polarize the cell and acquire its impedance over a wide range of frequencies, a variable frequency voltage source is necessary.

An Arduino Due microcontroller board was used to implement a Digital Direct Synthesis (DDS) technique. This converts digital numbers stored in an array into analogue signals through conversions executed by a Digital-to-Analogue Converter (DAC). It processes data blocks read from a look-up table in a Static Random-Access Memory (SRAM) to generate a form of frequency-tunable and phase-tunable output signal with reference to a fixed frequency precision clock source [7].

With the introduction of a phase accumulator function into the digital signal chain, this architecture becomes a numerically-controlled oscillator, now being able to alter the frequency of the output sinwave, according to a pre-defined specific range of frequencies.

C. Band-pass Filter

An active band-pass filter is required to exclusively select frequencies inside the 0.01Hz-10kHz spectrum, as this range fully describes the battery cell behaviour. A lower cut-off frequency of 0.01Hz is essential, this way filtering the DC offset included in the signal generated by the Arduino Due DAC.

There are some filter specifications: it requires a Butterworth response due to its nearly flat pass band with unity gain and no ripple, this way obtaining a uniform frequency response for all the wanted frequencies. The architecture that will be used is the Sallen-Key owing to its ability to operate under unity amplifier gain. The Sallen-Key topology has a low-pass or high-pass roll off 20dB/dec for every pole. Thus, an eight order Butterworth Band-pass filter will have an attenuation rate of -80dB/dec and 80 dB/dec. Such solution is recommended for this application, forming an eight-order Butterworth Band-pass filter after cascading two stages of second-order low-pass filters with two stages of second-order high-pass filters [8].

Table I lists the specifications for the desired Band-pass filter.

Lower Cut-Off Frequency	10mHz
Higher Cut-Off Frequency	10kHz
Centre Frequency	10Hz
Band-pass Gain	1

TABLE I: Filter Specifications.

1) 4th Order Unity-Gain Sallen-Key Low-Pass Filter: For a given C_1, C_2, C_3 and C_4, the resistor values for R_1, R_2, R_3, R_4 are determined by:

$$R_{1,2} = \frac{a_1 C_2 \mp \sqrt{a_1^2 C_2^2 - 4 b_1 C_1 C_2}}{4\pi f_c C_1 C_2} \tag{5}$$

$$R_{3,4} = \frac{a_2 C_4 \mp \sqrt{a_2^2 C_4^2 - 4 b_2 C_3 C_4}}{4\pi f_c C_3 C_4} \tag{6}$$

Where a_1, b_1, a_2 and b_2 are the coefficients associated with each second order polynomial, considering a fourth-order Butterworth filter type.

C_2 and C_4 must satisfy the following condition, so that real values for values for R_1, R_2, R_3 and R_4 are obtained:

$$C_2 \geq C_1 \frac{4b_1}{a_1^2} \tag{7}$$

$$C_4 \geq C_3 \frac{4b_2}{a_2^2} \tag{8}$$

Considering the higher cut-off frequency, f_c of 10kHz, the following values are obtained:

R values [Ω]		C values [F]	
R_1	47.4k	C_1	100p
R_2	240k	C_2	220p
R_3	35.7k	C_3	100p
R_4	86.6k	C_4	820p

TABLE II: Values for the low-pass filter components.

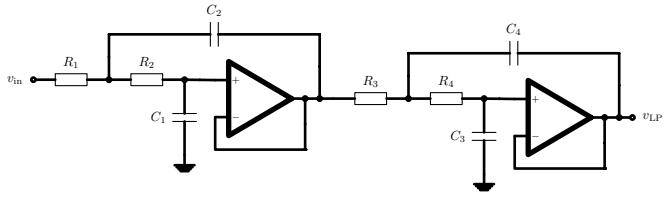

Fig. 3: 4th Order Unity-Gain Sallen-Key Low-Pass Filter.

2) 4th Order Unity-Gain Sallen-Key High-Pass Filter: For a certain value of C_5 and C_6, R_5, R_6, R_7 and R_8 are calculated for a low cut-off frequency, f_c:

$$R_5 = \frac{1}{\pi f_c C_5 a_1},\ R_6 = \frac{a_1}{4\pi f_c C_5 b_1} \tag{9}$$

$$R_7 = \frac{1}{\pi f_c C_6 a_2},\ R_8 = \frac{a_2}{4\pi f_c C_6 b_2} \tag{10}$$

Again, for a fourth-order Butterworth filter type, a_1, b_1, a_2 and b_2 represent the coefficients associated with each second order polynomial.

Considering the lower cut-off frequency of 10mHz, the following values are obtained:

R values [Ω]		C values [F]	
R_5	1.74M	C_5	10μ
R_6	1.47k	C_6	10μ
R_7	4.53M		
R_8	619k		

TABLE III: Values for the high-pass filter components.

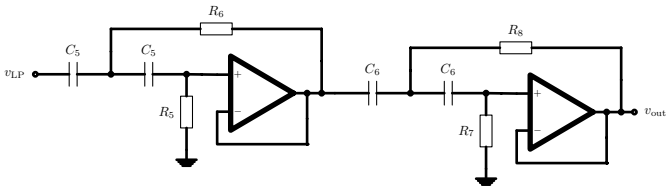

Fig. 4: 4th Order Unity-Gain Sallen-Key High-Pass Filter.

D. Enhanced Howland Current Source

A current source based excitation system is proposed due to the low impedance value of the tested $LiFePO_4$ cell (internal impedance is specified as less than 1 mΩ at 1 kHz in the $LiFePO_4$ datasheet). The maximum output current from an Arduino Due DAC is 15 mA. Therefore, a current amplifier is required in order to generate a greater voltage response from the cell. An enhanced Howland current source is chosen since it can be constructed using a single operational amplifier and five resistors.

The Howland circuit is modelled as a linear voltage-controlled current source (VCCS). The model is driven by an external and independent voltage source that drives the VCCS input, in this case, the variable frequency voltage source at the output of the filter [11].

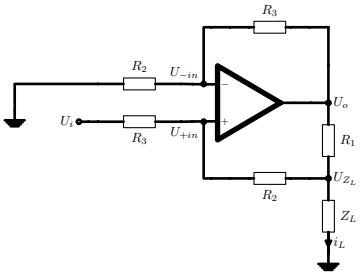

Fig. 5: Enhanced Howland Current Source.

Considering an infinite open-loop voltage gain, A_d, of the operational amplifier, the following equation is written, by current analysis:

$$I_L = \frac{U_i}{R_1} + (\frac{R_2 - R_3}{R_1 R_3} - \frac{1}{R_2 + R_3})U_{Z_L} \tag{11}$$

According to (11), one can conclude that for a high value of both R_2 and R_3, while imposing $R_2 = R_3$, the output current is very close to be independent from the load impedance. Therefore, the equation (11) for the output current, simplifies to:

$$I_L \approx \frac{U_i}{R_1} \tag{12}$$

An enhanced Howland current source was designed to generate a 2 A_{p-p} sinusoidal current. A 2 V_{p-p} voltage signal was applied to the circuit as input, with R_2 = R_3 = 10 kΩ and R_1 = 1 Ω. Hence, in order to apply to the terminals of the cell a 2 A_{p-p} sinusoidal current, a high-current operational amplifier is required. An OPA548 from Texas Instruments was

the choice considering that it allows the output current limit to be adjusted from 0 A to 5 A.

E. Data Acquisition

A second Arduino is used to read the sinusoidal current imposed to the cell and its voltage response.

In order to precisely acquire lower voltage and current increments, particularly relevant in this project due to the low impedance of the cell, a higher resolution than the 12 bit integrated ADC input of the Arduino is required. Hence, the approach of using two external AD7680 (by Analog Devices) ADCs, having a 16 bit resolution, was taken. One for the voltage at the cell terminals, the other for the voltage output of the current transducer. The current is measured by a LEM hall effect transducer current sensor (LTSR 6-NP). It measures bi-directional currents up to 6 A RMS from DC to 200 kHz.

Both voltage and current are sampled and, after the analog to digital conversion, the sequence of digital words is later stored in the Arduino Due 96 KBytes SRAM. Due to the memory limitation, one can only afford to store a finite number of digital words when sampling the variable frequency signals. Due to memory limitation, one can only afford to store a finite number of digital words when sampling the variable frequency signals. Given this limitation, it was chosen to store 320 samples for each of the frequencies. To attain this, the Arduino responsible for acquiring the signals requires the value of the frequency of the sinusoidal current being imposed to the cell during the acquisition interval. This is achieved by creating a communication channel via I2C protocol between the Arduino in charge of generating the variable-frequency AC voltage signal and the Arduino responsible for the data acquisition. Follow, the sampling frequency is calculated so that only 320 samples during each acquisition time window (five complete cycles of the generated signal) are acquired.

The process of signal acquisition in this project requires a fine resolution due to the small fluctuations in the sampled voltage and current signals. One way to increase the resolution of the ADC output is by oversampling and averaging functions. In this project, each sample is oversampled 80 times and later the accumulated value is divided by this value, giving the ADC resolution an increment of 6 bits, so, instead of 16 bits as previously, both ADCs now have 22 bits of resolution.

In order to further improve the random noise reduction achieved by the oversampling and averaging process, a moving average filter is implemented, this way reducing random white noise while maintaining a sharp step response. In this project, a 22 point moving average filter is applied to both voltage and current acquired signals, reducing the random noise by a factor of 4.7.

The Discrete Fourier transform (DFT) is the chosen method to estimate both voltage and current phasors. After sampling, stored data at discrete time step is available for processing. Hence, the Fourier-transform calculation has been performed in discrete environment and is named as Discrete Fourier Transform or DFT [9]. The discrete Fourier transform of a general sequence $x[n]$ of finite duration is determined as follows [10]:

$$X(m) = \sum_{n=0}^{N-1} x(n) e^{-j2\pi nm/N} \tag{13}$$

where $x(n)$ is a discrete sequence of time-domain sampled values of the continuous variable $x(t)$; n is the time-domain index of the input samples; N is the number of samples of the input sequence and the number of frequency points in the DFT output; m is the index of the DFT output in the frequency domain, equivalent to the number of complete cycles that occur over the N points of the signal.

A sinusoid $x(t)$ with frequency mf_0 with a Fourier series:

$$x(t) = a_m \cos(2\pi m f_0 t) + b_m \sin(2\pi m f_0 t) = \tag{14}$$

$$= \sqrt{a_m^2 + b_m^2}\, \cos(2\pi m f_0 t + \phi) \tag{15}$$

has a phasor representation as follows:

$$\overline{X(m)} = \sqrt{a_m^2 + b_m^2}\, e^{j\phi}, \tag{16}$$

$$\phi = \arctan(-\frac{b_m}{a_m}) \tag{17}$$

The phasor in its complex form becomes:

$$\overline{X(m)} = a_m - j b_m \tag{18}$$

Likewise, when applying Euler's formula to equation (13), the phasor representation of the mth harmonic component is equivalent to:

$$\overline{X(m)} = \sum_{n=0}^{N-1} x(n)[\cos(2\pi nm/N) - j\sin(2\pi nm/N)] \tag{19}$$

If we define the cosine and sine sums as follows:

$$\overline{X_c(m)} = \sum_{n=0}^{N-1} x(n)\cos(2\pi nm/N), \tag{20}$$

$$\overline{X_s(m)} = \sum_{n=0}^{N-1} x(n)\sin(2\pi nm/N), \tag{21}$$

then the phasor $X(m)$ is given by:

$$\overline{X(m)} = \overline{X_c(m)} - j\overline{X_s(m)} \tag{22}$$

A 4-cycle DFT considers a window size of:

$$N = 4\frac{fs}{fn} \tag{23}$$

Which is four times greater that considering only one cycle. This yields to an attenuation of high and low frequency harmonics, significantly improving the output results of both voltage and current phasor estimation, for each frequency. The reason behind a better resolution when acquiring more cycles is that it decreases the effect of spectral leakage, a phenomena associated with the non-cyclical input of the Fourier-transform.

Processing more than one cycle is a good practice since it increases the number of complete cycles in the sampled interval, reducing the effect of leakage but still does not fully

solves the leakage problem. In this project, with the purpose of reducing the spectral leakage effect in both voltage and current phasor estimation, a technique known as windowing was applied. Windowing works by selecting the DFT input data in order to reduce the non-integer number of cycles over the N samples interval. This was achieved with a rectangular window, leading to a grater attenuation of high and low frequency harmonics in the DFT output.

Employing the DFT algorithm to both voltage and current samples, we obtain the impedance for each frequency k:

$$\overline{Z_k(m)} = |Z_k(m)|e^{j\phi_{Z_k}} \tag{24}$$

where the impedance magnitude of the mth harmonic, $|Z_k(m)|$ and phase angle of the impedance, $\phi_{Z_k}(m)$ are obtained as follows:

$$|Z_k(m)| = |\frac{U_k(m)}{I_k(m)}| = \frac{\sqrt{U_{k_c}(m)^2 + U_{k_s}(m)^2}}{\sqrt{I_{k_c}(m)^2 + I_{k_c}(m)^2}} \tag{25}$$

$$\phi_{Z_k}(m) = \arctan(-\frac{U_{k_s}(m)}{U_{k_c}(m)}) - \arctan(-\frac{I_{k_s}(m)}{I_{k_c}(m)}) \tag{26}$$

F. Adaptive Neuro Fuzzy Inference Systems applied to SOC estimation

The impedance spectra for each SOC is obtained through the previous EIS measurement system. This way, an adaptive neuro-fuzzy inference system that uses two input variables has been implemented. The input variables are the real part of the measured complex impedance and its imaginary part. The output of the ANFIS system will be the battery cell inferred SOC. The estimation of the battery SOC will be achieved through a comparative analysis of its actual impedance spectra with the impedance spectra database previously built from past EIS measurements for pre-defined SOC values.

Both inputs, real and imaginary impedance parts, are mapped to their own membership functions using the Fuzzy Logic Toolbox function existent in MATLAB. Instead of triangular membership functions, Gaussian ones will be used. The Gaussian function, represented in Figure , expressed in equation 5.1, is specified with two parameters, m and σ, as follows:

$$f(x, m, \sigma) = e^{-\frac{(x-m)^2}{\sigma^2}} \tag{27}$$

where m denote the mean value, corresponding to the centre of the function, and σ, the standard deviation, giving its width.

To properly distinguish the different SOC EIS measurements, each one having N different points, N representing the number of different frequencies in the frequency sweep, the model requires a certain number of IF-THEN rules in order to differentiate the precessed data. The necessary number of rules providing an accurate system is approximately half the total number of impedance data points stored in the database. The database will be composed by M impedance spectras, one for each pre-defined SOC. Each impedance spectra contains N points, one for each frequency, and each of these points is defined by its real value and imaginary value. Hence, the total number of rules comes:

$$N_{rules} = \frac{M_{SOCs} \cdot N_{frequencies} \cdot N_{inputs}}{2} \tag{28}$$

In this project, the so-called Sugeno, or Takagi-Sugeno-Kang, method of fuzzy inference, mapped over a neural network structure is applied. This methodology uses a linear or constant level as the output membership function rather than a distributed fuzzy set. This is known as a singleton output membership function, ω.

After running the Fuzzy Logic Toolbox function, a FIS file is given as output, modelling the Sugeno fuzzy inference model, containing the membership function parameters for both real and imaginary impedance parts inputs and the first-order polynomial parameters, describing the output singleton membership functions.

Following the modelling process, the fuzzy inference system is implemented in the acquisition Arduino Due, setting the IF-THEN rules, where the subsets of each rule are described by their membership functions, characterized by the tailored parameters computed by the neuro-adaptive technique and displayed in the FIS file. The combination of input membership functions and singleton outputs for each input variable results in different rules of the system:

Rule 1: If Re(Z) is $\mu^{(1)}_{Re(Z)}$ and $-Im(Z)$ is $\mu^{(1)}_{-Im(Z)}$,
then $\omega^{(1)} = m_1 Re(Z) + n_1(-Im(Z)) + k_1$

Rule 2: If Re(Z) is $\mu^{(2)}_{Re(Z)}$ and $-Im(Z)$ is $\mu^{(2)}_{-Im(Z)}$,
then $\omega^{(2)} = m_2 Re(Z) + n_2(-Im(Z)) + k_2$

Rule 3: If Re(Z) is $\mu^{(3)}_{Re(Z)}$ and $-Im(Z)$ is $\mu^{(3)}_{-Im(Z)}$,
then $\omega^{(3)} = m_3 Re(Z) + n_3(-Im(Z)) + k_3$

$\vdots$

Rule N: If Re(Z) is $\mu^{(N)}_{Re(Z)}$ and $-Im(Z)$ is $\mu^{(N)}_{-Im(Z)}$,
then $\omega^{(N)} = m_N Re(Z) + n_N(-Im(Z)) + k_N$

Figure 6 shows the reasoning mechanism for the Sugeno model applied to the SOC estimation. This process is implemented in the acquisition Arduino, automatically inferring the SOC for each of the N frequency points in the EIS current measured impedance spectra.

In layer 1, every node is an adaptive node with a node function equal to the membership function, for which the parameters $m^{(i)}$ and $\mu^{(i)}$, characterizing each gaussian membership function, have been estimated by means of the Fuzzy Logic Toolbox function.

Afterwards, the singleton output of each rule, $\omega^{(i)}$, is weighted by the firing strength of the rule, $f^{(i)}(Re(Z), -Im(Z))$ for both inputs, $Re(Z)$ and $-Im(Z)$.

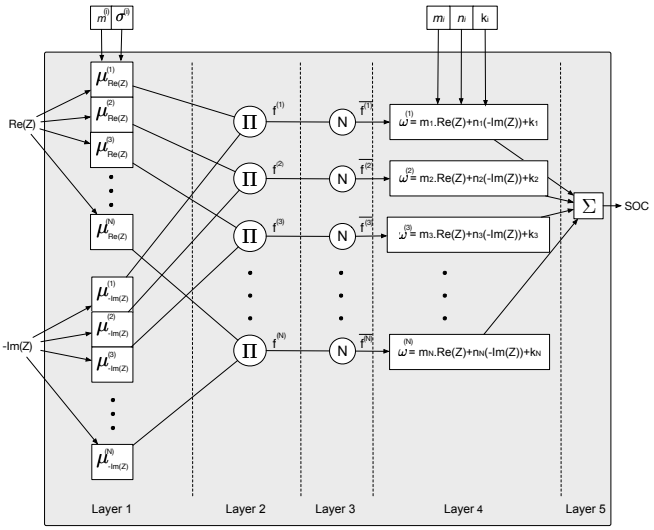

Fig. 6: Structure of the five-layer adaptive neuro-fuzzy system for the Sugeno model implemented in the acquisition Arduino Due.

This is performed in layer 2, where each node is fixed, representing the firing strength associated to each rule i:

$$f^{(i)}(Re(Z), -Im(Z)) = \mu^{(i)}_{Re(Z)}(Re(Z)) \cdot \mu^{(i)}_{-Im(Z)}(-Im(Z)) \tag{29}$$

where $\mu^{(i)}_{Re(Z)}(Re(Z))$ and $\mu^{(i)}_{-Im(Z)}(-Im(Z))$ are the values of degrees of membership for the rule i relative to both inputs.

In layer 3 each node is fixed. Now the incoming firing strength is normalized to the sum of all rules firing strengths:

$$\overline{f^{(i)}(Re(Z), -Im(Z))} = \frac{f^{(i)}(Re(Z), -Im(Z))}{\sum_{k=1}^{N} f^{(k)}(Re(Z), -Im(Z))} \tag{30}$$

where N represents the total number of rules, given by expression (28).

In layer 4 each node is adaptive. At this point, the firing rules are multiplied by their correspondent singletons, for which the parameters m_i, n_i and k_i , characterizing each output singleton, have been estimated through the Fuzzy Logic Toolbox function.

$$\overline{f^{(i)}(Re(Z), -Im(Z))} \cdot \omega^{(i)} = \overline{f^{(i)}(Re(Z), -Im(Z))} \cdot (m_i Re(Z) + n_i(-Im(Z)) + k_i) \tag{31}$$

Layer 5 is composed by a single fixed node, computing the SOC value output as the sum of all incoming signals, representing the centre of gravity or the weighted average of all rule outputs:

$$SOC = \sum_{k=1}^{N} (\overline{f^{(i)}(Re(Z), -Im(Z))} \cdot \omega^{(i)}) = \frac{\sum_{k=1}^{N} (f^{(l)}(Re(Z), -Im(Z)) \cdot \omega^{(i)})}{\sum_{k=1}^{N} f^{(i)}(Re(Z), -Im(Z))} \tag{32}$$

IV. Results

This chapter aims the validation of the implemented EIS measurement system and Fuzzy logic SOC inference method. It presents information and results about both processes with the aid of a case study considering a 160 Ah capacity $LiFePO_4$ cell having a 70% SOC.

V. Assumptions

In order to run the above mentioned and implemented techniques, the following listed premises were defined so that some of the variables affecting the battery cell impedance were controlled:

- Temperature: During the experiments, the battery cell was maintained at a room temperature of 17 C with a temperature fluctuation of $\pm$ 1C.
- Relaxation Time: After each battery cell discharge, the resting time of the cell was established as 10 minutes.
- Charge/Discharge rates: The cell was charged at a rate of 7.4 Ah and discharged at a rate of 16 Ah.
- Operating Voltages: The impedance spectra of the cell was measured galvanostatically in a voltage range between 2.8 and 3.6 V, corresponding to 15% and 100% SOC, respectively.
- Impedance database: Generated during one full discharge cycle (100% - 15%). The battery cell was later fully charged again and discharged to certain SOC's to present the reader the proposed case studies.

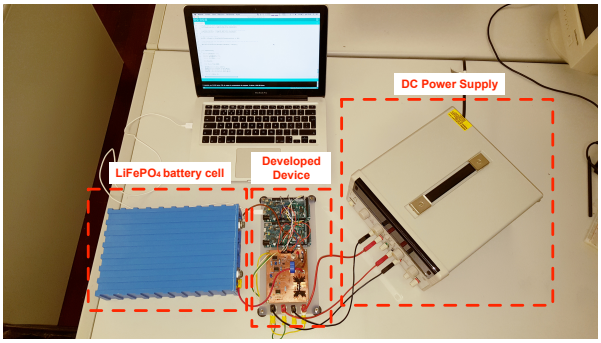

Fig. 7: Experimental scenario.

A. Validation of the EIS measurement system implementation

The variable frequency voltage source provided by the Digital Direct Synthesis (DDS) technique in the source Arduino Due was programmed with a 2000 digital word look-up table, supplying at the output of the Arduino DAC a voltage with a duration of six complete cycles, as follows:

$$U_{DAC}(t) = U_{o_{AC}} \sin(2\pi f_i t + \varphi) + U_{o_{DC}} \quad [\text{V}] \tag{33}$$

where $U_{o_{AC}} = U_{o_{DC}} = 1.6114\ V$; $\varphi = \frac{\pi}{6}\ rad$ and a variable frequency value f_i, so that the frequency sweep is carried, for each of the following values:

After the filtering stage, this voltage is then presented to the dimensioned Enhanced Howland Current Source so that

Frequency (Hz)							
f_1	0.0130	f_7	0.0750	f_{13}	0.4220	f_{19}	2.3720
f_2	0.0180	f_8	0.1000	f_{14}	0.5630	f_{20}	3.1590
f_3	0.0237	f_9	0.1330	f_{15}	0.7500	f_{21}	4.1780
f_4	0.0316	f_{10}	0.1800	f_{16}	1.000	f_{22}	5.6340
f_5	0.0422	f_{11}	0.2370	f_{17}	1.3390		
f_6	0.0563	f_{12}	0.3160	f_{18}	1.7680		

TABLE IV: Programmed frequencies in the variable frequency voltage source Arduino Due, for which the EIS measurement system was realized.

accordingly to equation (12), an excitation current is imposed to the battery cell:

$$I_L(t) \approx \frac{U_{out_{Filter}}(t)}{R_1} = \frac{1.6114\sin(2\pi f_i t + \frac{\pi}{6})}{1} = 1.6114\sin(2\pi f_i t + \frac{\pi}{6})\ [A] \tag{34}$$

Both voltage and current are sampled at a sampling frequency dependent on that transmitted from the source Arduino, presented in table V, to the acquisition one, via I2C communication. The acquisition arduino is programmed in order to store 320 samples for each one of the 22 frequencies in table V so that approximately 280 samples are correctly acquired during 5 complete cycles, while oversampling and digital filtering the current samples. As an example, the acquired voltage at the terminals of the cell and excitation current signals, after oversampling and applying the digital filter, for a frequency of 0.0422Hz, are presented in Figure 8 (a) and 8 (b), respectively.

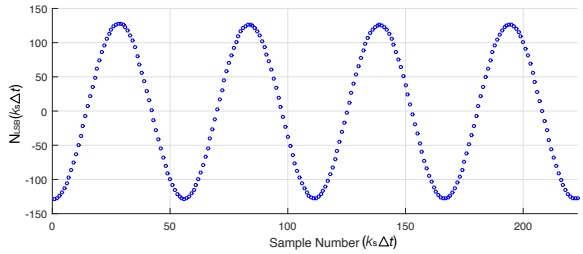

(a)

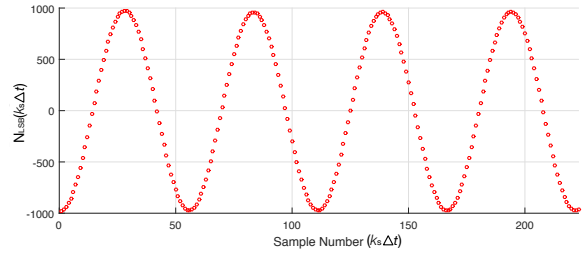

(b)

Fig. 8: Acquired voltage at the terminals of the cell and excitation current signals for a frequency of 0.0422Hz: (a) Voltage sequence before windowing; (b) Current sequence before windowing; (c) Voltage sequence after windowing; (d) Current sequence after windowing

Now the DFT algorithm to both windowed voltage and current samples for each of the frequencies in table V is applied, thus obtaining the phasors for each of the variables. Afterwards, each digital word contained in the stored voltage and current arrays is converted back to its units.

The impedance data assessed through the acquired voltage and current phasors is represented through a Nyquist plot, expressing the imaginary impedance versus the real impedance of the system in Figure 9.

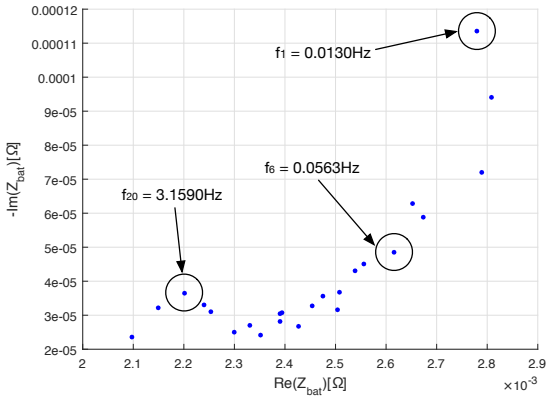

Fig. 9: Nyquist plot of the impedance data assessed through the acquired voltage and current phasors for a 160 Ah battery cell with 70% SOC.

The same process is executed to the following values of SOC during a discharge cycle so that a database to the fuzzy inference system is constructed:

SOC(%)	100	90	80	70	60	50	40	30	20	15

TABLE V: Pre-defined SOC's for which the impedance spectra database has been composed.

The obtained impedance spectra database is graphically presented in Figure 10 and Figure 11.

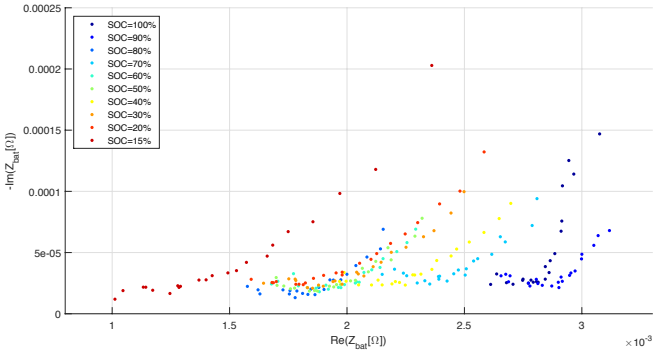

Fig. 10: Nyquist plot of the impedance spectra database for the referred SOC's in table V.

A fuzzy system that accurately distinguishes the different SOC EIS measurements, each with 22 points, requires a certain number of rules in order to differentiate, with enough precision, the precessed data.

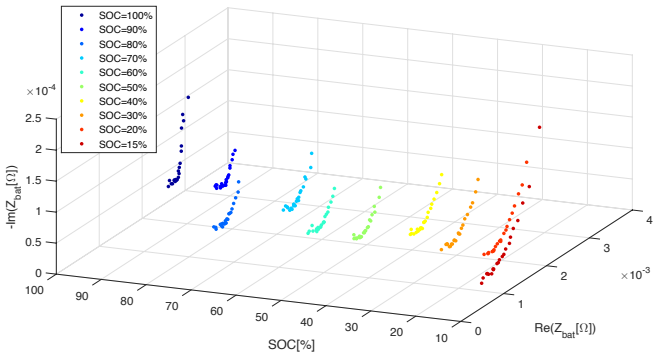

Fig. 11: Nyquist plot of the impedance spectra database as function of the referred SOC's in table V.

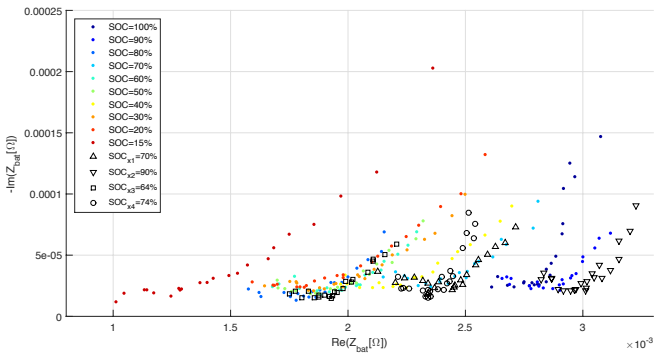

Fig. 12: Nyquist plot of the impedance spectra database and the acquired impedance spectra for each of the presented case studies.

The necessary number of rules providing an accurate system is approximately half the total number of impedance data points stored in the database. The database is composed by 10 impedance spectras, one for each SOC. Each impedance spectra contains 22 points, one for each frequency, and each of these points is defined by its real value and imaginary value. Hence, the total number of rules comes:

$$N_{rules} = \frac{N_{SOC's} \cdot N_{frequencies} \cdot N_{inputs}}{2} = \frac{10 \cdot 22 \cdot 2}{2} = 220 \tag{35}$$

Each subset of rules (i.e. both fuzzy inputs and output) can be represented by its own membership function, thus, there are 220 gaussian membership functions for each input (Re(Z) and -Img (Z)) and 220 output membership functions (singleton output membership functions) modelling the database.

B. Validation of the Fuzzy Logic SOC inference system

The impedance spectra database is initially evaluated and the rule base is constructed.

After creating the database and consequent system rule base, in order to validate the fuzzy logic SOC inference system, four measurements were performed. The battery was fully recharged again, and later discharged so that the system could be tested to a SOC value of 90%, 70%, 74% and 64%. The obtained results from the EIS measurement system are presented in Figure 12, together with the pre-acquired database, where the impedance spectra points are marked as △ for 70%, ▽ for 90%, □ for 64% and ○ for a 74% SOC value.

The fuzzy system inferred SOC outputs for each of the four input profiles (marked by red asterisks), can be observed in Figures 13 (90%), 14 (70%), 15 (74%) and 16 (64%). The output average of the 22 estimated points is represented by a red marker (◊) in each plot.

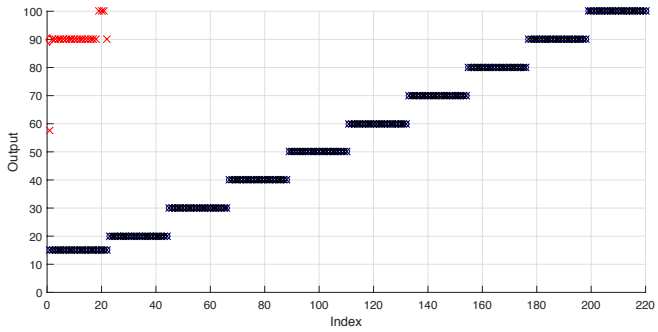

Fig. 13: Fuzzy system output(marked by red asterisks) for the battery cell with a 90% SOC value. The output average of the inferred points is marked as ◊.

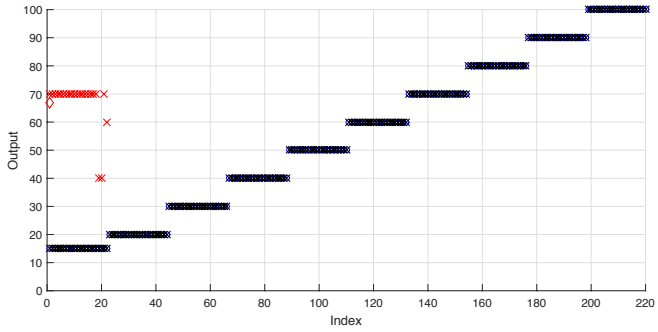

Fig. 14: Fuzzy system output(marked by red asterisks) for the battery cell with a 70% SOC value. The output average of the inferred points is marked as ◊.

Table VI displays the average and variance values of the four case studies output results. Analysing the table, it is evident that concerning input values with a SOC value not included in the modelling of the fuzzy system, in other words, for impedance spectras having a SOC value not included in the impedance spectra database, the average value of the output points is a random value and the corresponding variances are high, portraying the spread out between the inferred output points, observed in the respective plots.

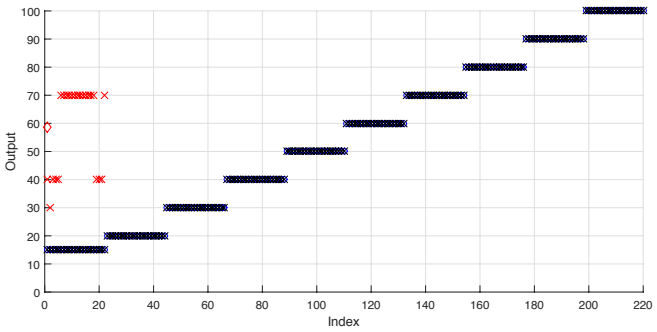

Fig. 15: Fuzzy system output(marked by red asterisks) for the battery cell with a 74% SOC value. The output average of the inferred points is marked as ◊.

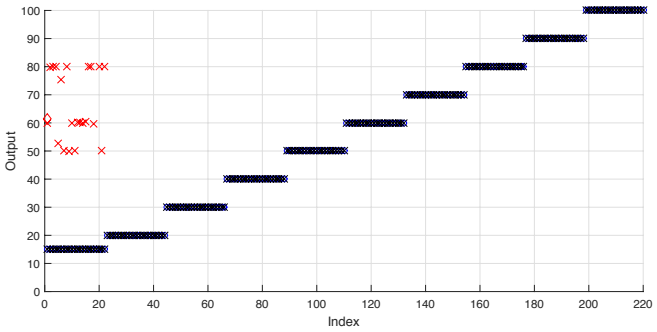

Fig. 16: Fuzzy system output(marked by red asterisks) for the battery cell with a 64% SOC value. The output average of the inferred points is marked as ◊.

As for the input values with a SOC value residing in the database, the output average is close to the expected value, presenting a lower variance, thus concluding that the system is able to estimate the current SOC of the battery cell, if the measured impedance spectra has a SOC value predefined in the constructed database.

Input	Output average	Output variance
Re(Z) and -Img (Z) of the cell with 90% SOC	89.88	64.57
Re(Z) and -Img (Z) of the cell with 70% SOC	66.82	79.88
Re(Z) and -Img (Z) of the cell with 74% SOC	58.64	240.91
Re(Z) and -Img (Z) of the cell with 64% SOC	61.53	606.56

TABLE VI: Output average and variance of the Fuzzy system for the proposed case studies.

VI. Conclusion

This work aimed the development of a system capable of automatically measuring the SOC value of a $LiFePO_4$ battery cell.

The developed device is capable of measuring the impedance profile of a given $LiFePO_4$ cell, performing an EIS measurement. The impedance profile assessed is afterwards used to infer its SOC value using an ANFIS based method. In order to implement this adaptive method, past impedance spectras, related to specific SOCs, constructed a database so that a valid fuzzy inference model is obtained. With this, a comparative analysis between the current cell's impedance and previous observed ones, using the considered fuzzy inference system (representing the non-linear behaviour of the internal impedance), yields the object of this thesis, the SOC value.

The device was validated for a 160 Ah $LiFePO_4$ cell, for the conditions listed in section V, and the obtained results provided substantial information to access its performance. It was verified that that the way the inference system is modelled defines the accuracy of the SOC estimation method. The fuzzy inference system, modelling the cell's impedance as function of the SOC value, was obtained considering ten pre-defined SOC values. It was demonstrated that the developed device is capable of estimating future SOC values for inferred values matching those present in the database. For intermediate values it was concluded that the inferred results average was a random value and its corresponding variances were quite high due to large variations between impedance spectras, as expected, justified by the non-linear behaviour of the $LiFePO_4$ cell's impedance in relation to SOC. With this in mind, for this device to properly work for the entire range of SOC values, including the intermediate ones, it is necessary to increase the number of acquired impedance spectras modelling the fuzzy inference system, i.e., increasing the number of pre-defined SOC values composing the database.

The conditions listed in section V concern a fixed operating temperature, only one charge/discharge cycle for the cell and a resting time of 10 minutes. Outside these conditions, the inferred SOC value is uncertain, seeing that the effects of each one of these variables in the cell's impedance were not taken into account in the course of this work.

References

[1] D. Linden. Handbook of batteries. McGraw-Hill, 1995.

[2] N. Watrin, B. Blunier, and A. Miraoui. Review of adaptive systems for lithium batteries stateof- charge and state-of-health estimation. In Transportation Electrification Conference and Expo (ITEC), 2012 IEEE, pages 16. IEEE, 2012.

[3] V. Prajapati, H. Hess, E. J. William, V. Gupta, M. Huff, M. Manic, F. Rufus, A. Thakker, J. Govar, et al. A literature review of state of-charge estimation techniques applicable to lithium poly-carbon monoflouride (li/cfx) battery. In Power Electronics (IICPE), 2010 India International Conference on, pages 18. IEEE, 2011.

[4] M. Fathi. Integrated Systems: Innovations and Applications. Springer Science & Business Media, 2015.

[5] P. Notten, H. Bergveld, andW. Kruijt. Battery Management Systems: Design by modelling. Springer Science & Business Media, 2002.

[6] J.-S. R. Jang, C.-T. Sun, and E. Mizutani. Neuro-fuzzy and soft computing: a computational approach to learning and machine intelligence. Prentice Hall, 1997.

[7] P. O. Olabisi and B. Olufeagba. Simplified analogue realization of the digital direct synthesis (dds) technique for signal generation. IOSR Journal of Electrical and Electronics Engineering (IOSRJEEE), 9(2):8589, 2014.

[8] M. Z. M. M. Myo, Z. M. Aung, and Z. M. Naing. Design and implementation of active band-pass filter for low frequency rfid (radio frequency identification) system. In Proceedings of the International MultiConference of Engineers and Computer Scientists, volume 1. Citeseer, 2009.

[9] A. G. Phadke and J. S. Thorp. Synchronized phasor measurements and their applications. Springer Science & Business Media, 2008.
[10] A. Oppenheim and A. Willsky. Signals and Systems. PrenticeHall, 1997.
[11] A. Tucker, R. Fox, and R. Sadleir. Biocompatible, high precision, wideband, improved howland current source with lead-lag compensation. Biomedical Circuits and Systems, IEEE Transactions on, 7(1):6370, 2013.